Materials Science and Engineering A 534 (2012) 83–89

Contents lists available at SciVerse ScienceDirect

Materials Science and Engineering A

journal homepage: www.elsevier.com/locate/msea

Alloying behavior in multi-component AlCoCrCuFe and NiCoCrCuFe high entropy alloys

S. Praveen, B.S. Murty, Ravi S. Kottada*

Department of Metallurgical and Materials Engineering, Indian Institute of Technology Madras, Chennai-600036, India

ARTICLE INFO

Article history:
Received 2 September 2011
Received in revised form 3 November 2011
Accepted 21 November 2011
Available online 28 November 2011

Keywords:
High entropy alloys
Nanostructured materials
Mechanical alloying
Ordering
Hardness measurement
X-ray diffraction

ABSTRACT

Multi-component high entropy alloys (HEAs) are observed to form simple solid solutions in contrary to general perception that complex compounds may form in such multi-component equi-atomic alloys. In the present study, alloying behavior was investigated using XRD in AlCoCrCuFe and NiCoCrCuFe equi-atomic high entropy alloys synthesized by mechanical alloying (MA) and spark plasma sintering (SPS). Simple FCC and BCC phases evolved after MA, while Cu-rich FCC and sigma (σ) phases evolved along with FCC and BCC phases after SPS. Further, NiCoCuFe, NiCoCrFe and NiCoFe equi-atomic alloys were investigated to confirm the formation of Cu-rich FCC, and σ phases. The hardness was observed to be 770 ± 10 HV for AlCoCrCuFe and 400 ± 10 HV for NiCoCrCuFe. Phase evolution after MA and SPS indicate that configurational entropy is not sufficient enough to suppress the formation of Cu-rich FCC, and σ phases, and enthalpy of mixing appears to play an important role in determining the phase formation in high entropy alloys after sintering.

1. Introduction

In general, structural materials that are currently available for most of the applications are based on single principle elements viz. Fe-based steels, Al-based alloys, Ni-based superalloys, etc. Although, solid solution strengthening by more than one solute in equi-molar proportion is a viable option, processing of alloys based on multi-principal elements was not attempted for a long time on the notion that they may form complex compounds with complex crystal structures. However, the first impressive report by Yeh et al. [1], followed by a few research groups [2–5], has emphatically shown that multi-component high entropy alloys (HEAs) can be processed to form simple solid solutions under appropriate conditions. The term "high entropy" in HEAs originates from the resultant high entropy of mixing (>1.61R, where R is gas constant) when more than five elements are mixed in equi-molar proportion. The HEAs formed with simple crystal structures have also exhibited interesting properties such as high room temperature strength, and strength retention at higher temperatures [1,2,5].

There have been several processing routes to prepare HEAs, viz., casting, sputtering, splat quenching, mechanical alloying (MA), and among those processes, HEAs prepared by casting route are widely studied. Although, HEAs prepared by casting nominally show simple solid solutions, detailed analyses have shown conclusively that casting route usually results in typical dendrite structure with some segregation in dendrite and inter-dendrite regions [3–7]. Similarly, metastable phases relative to casting are formed during splat quenching or sputtering method, and reported that these may become stable after annealing at high temperature [3]. On the contrary, HEAs formed via MA route appear to give more homogeneous and stable nanocrystalline microstructures [8–14]. Further, good densification characteristics and high hardness were observed for HEA synthesized by MA and spark plasma sintering (SPS) [13].

Based on the contradicting observations in the literature on alloying, the persistent question one needs to ask is whether solid solution criteria proposed for HEAs in the literature [15,16] are valid for MA route. It is also important to know why some single phase HEAs formed after MA, phase-separate (or precipitate other phases) during densification [12,13]. In order to address these issues, in the present study, equi-atomic AlCoCrCuFe, NiCoCrCuFe, NiCoCuFe, NiCoCrFe and NiCoFe were chosen for synthesis of HEAs by MA followed by densification. Alloying behavior of the above alloys during MA and after densification is studied by employing a detailed characterization via X-ray diffraction (XRD) and scanning electron microscopy (SEM).

2. Experimental details

Equi-atomic elemental blends of Al, Co, Cr, Cu, Fe, Ni powders with purity higher than 99.5% were mechanically alloyed to synthesize equi-atomic AlCoCrCuFe, NiCoCrCuFe, NiCoCrFe, NiCoCuFe

* Corresponding author. Tel.: +91 44 2257 4779; fax: +91 44 2257 4752.
E-mail addresses: spravin88@gmail.com (S. Praveen), murty@iitm.ac.in (B.S. Murty), ravi.sankar@iitm.ac.in, raviskottada@gmail.com (R.S. Kottada).

0921-5093/$ – see front matter © 2011 Elsevier B.V. All rights reserved.
doi:10.1016/j.msea.2011.11.044

and NiCoFe HEAs. FritshPulverisette-P5 high energy ball mill at a ball to powder weight ratio of 10:1 using hard chrome steel vials and balls was utilized for mechanical alloying. Ball milled powders were consolidated by SPS at 900 °C for 15 min at a pressure of 50 MPa. To study the alloying behavior during milling, powder samples were taken at a regular interval of 5 h and XRD experiments were carried out in Xpert Pro Panalytical instrument. Phase evolution after sintering was also studied by XRD. Hardness measurements were carried out on the consolidated samples at a load of 1 kg with dwell time of 10 s in Wilpert WilsonVicker's hardness instrument. The reported hardness measurements are an average of at least ten measurements done on both sides of the sample pellet. A SEM equipped with energy dispersive spectrometry (EDS) was used for phase identification and composition analysis of the phases. In order to verify the homogeneity of the dense pellets, SEM and hardness measurements were carried out on both sides of the pellet for each alloy system.

3. Results

The XRD, SEM micrographs and hardness measurements reported here are the representative results of a given composition. All the results (XRD, SEM and hardness) presented here are observed to be consistent on both sides of the pellets, and thus ensuring the homogeneity and uniformity of the dense pellets.

3.1. Phase evolution during MA

Fig. 1a and b represents the XRD patterns of the mechanically alloyed powders of AlCoCrCuFe and NiCoCrCuFe as a function of milling time, respectively. Major BCC (designated as B) phase and a minor FCC phase were observed in AlCoCrCuFe after 15 h of milling. A closer look at the peak positions of the minor FCC phase indicates that this FCC phase is Cu rich and has been designated as F_{Cu}. In contrast, Cu dissolves completely in NiCoCrCuFe, and a major FCC (designated as F) phase evolves together with minor BCC phase (designated as B_{minor}). It is clear from Fig. 1b that in NiCoCrCuFe, Ni peaks shift towards lower angles (towards Cu peaks) with milling time (compare the XRD of 10 min and 10 h milling) and the final FCC (F) phase peak positions are close to that of Cu.

Subsequently, the affinity for FCC phase formation was verified by choosing two different compositions, NiCoFe and NiCoCrFe without Cu, and another composition NiCoCuFe with Cu. Fig. 2a shows the XRD patterns of NiCoFe, NiCoCrFe and NiCoCuFe together with NiCoCrCrFe. Among these three alloys, NiCoFe and NiCoCuFe have shown single phase FCC (F) formation, while the Cr containing NiCoCrFe has shown a small amount of BCC phase (B_{minor}) along with FCC (F) on MA, which is clear from the asymmetry in the lowest angle XRD peak (Fig. 2a). Fig. 2b and c shows the first two XRD peaks of NiCoCrFe and NiCoCrCuFe in de-convoluted form, which illustrate that a minor BCC phase (B_{minor}) forms in Cr containing alloys.

It is interesting to note from the XRD patterns of NiCoCuFe and NiCoCrCuFe (Fig. 2a) that the FCC phase (F) peak positions are very close to those of Cu in both the alloys containing Cu. This observation suggests that all the other elements appear to be dissolving into Cu. Interestingly, XRD patterns of NiCoFe and NiCoCrFe show that the FCC (F) peak positions in these alloys are also same as in the alloys with Cu, though these alloys do not contain Cu. This clarifies that all other elements are dissolving in Ni and not in Cu and thus the peak shift of Ni is not because of formation of FCC (F) phase with Cu. It is also important to note that when Al replaces Ni to form an alloy such as AlCoCrCuFe (Fig. 1a), all the elements except Cu are observed to be dissolving into Fe or Cr and no shift in peaks was observed with milling time.

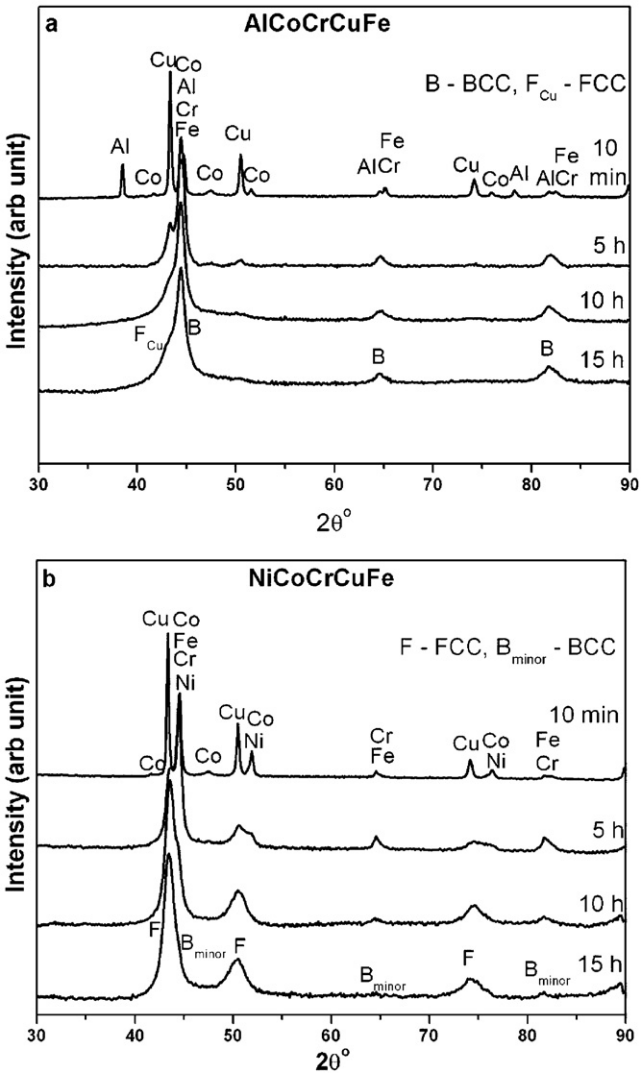

Fig. 1. XRD patterns of mechanically alloyed powders of (a) AlCoCrCuFe and (b) NiCoCrCuFe HEAs as a function of milling time.

3.2. Phase evolution due to densification by SPS

Fig. 3 shows the XRD pattern of AlCoCrCuFe and NiCoCrCuFe after SPS at 900 °C. A detailed analysis of the XRD pattern of AlCoCrCuFe after sintering illustrates that a major ordered BCC phase (B2), a Cu rich FCC phase (F_{Cu}), and minor sigma phase (σ) are visible. It is important to note that in contrast to only one BCC (B) phase with partial dissolution of Cu after 15 h ball-milling, additional phase (σ) evolved during sintering. The Cu is observed to segregate out as an FCC phase (F_{Cu}) and accordingly diffraction peaks corresponding to Cu are clearly visible.

Inset in Fig. 3 shows the prominent XRD peaks of NiCoCrCuFe in de-convoluted form illustrating the formation of two FCC phases (F_1 and F_2) after SPS. As compared to only one FCC phase (F) and a minor BCC (B_{minor}) after 15 h ball-milling in NiCoCrCuFe (Fig. 1b), two FCC phases (F_1 and F_2), and minor sigma phase (σ) are observed after SPS in NiCoCrCuFe (Fig. 3). Unlike AlCoCrCuFe, no ordered BCC (B2) phase was observed in NiCoCrCuFe after sintering. Fig. 4 shows the XRD pattern of NiCoFe, NiCoCrCuFe, NiCoCrFe, and NiCoCrCu after SPS at 900 °C; inset shows the de-convoluted form of XRD peaks. Formation of the second FCC phase (F_2) in Cu containing systems (NiCoCuFe, NiCoCrCuFe, AlCoCrCuFe) indicates that the presence of Cu led to the segregation of second FCC phase (F_2). Absence of minor

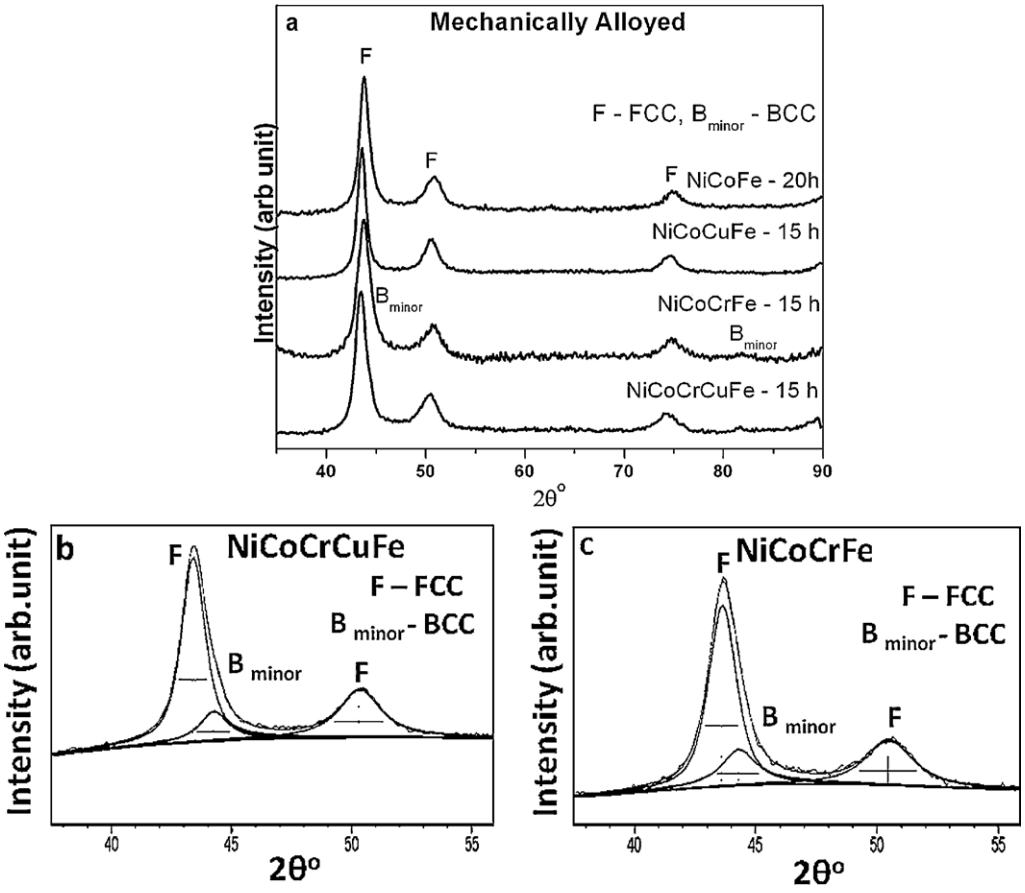

Fig. 2. (a) XRD patterns of mechanically alloyed HEAs, (b) and (c) enlarged part of XRD patterns showing de-convoluted peaks.

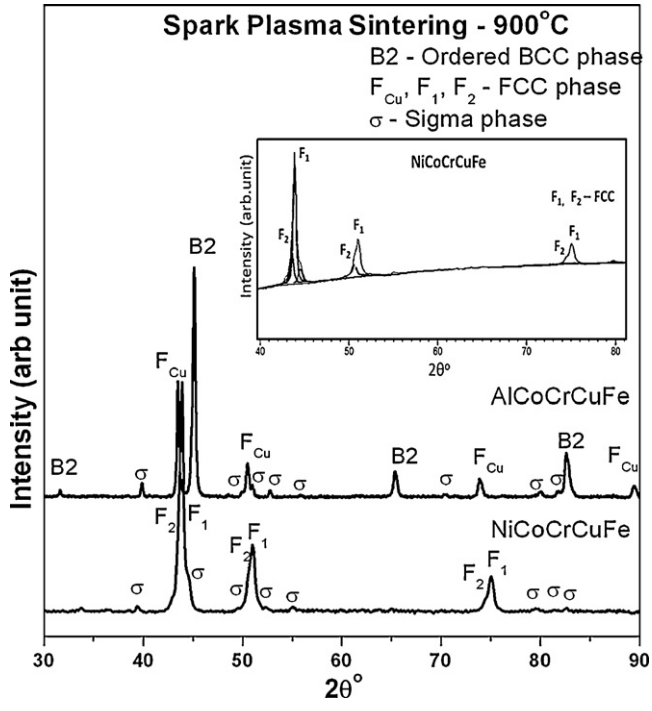

Fig. 3. XRD patterns of AlCoCrCuFe and NiCoCrCuFe after SPS. Inset shows the de-convoluted form of XRD peaks of NiCoCrCuFe showing the formation of F_1 and F_2.

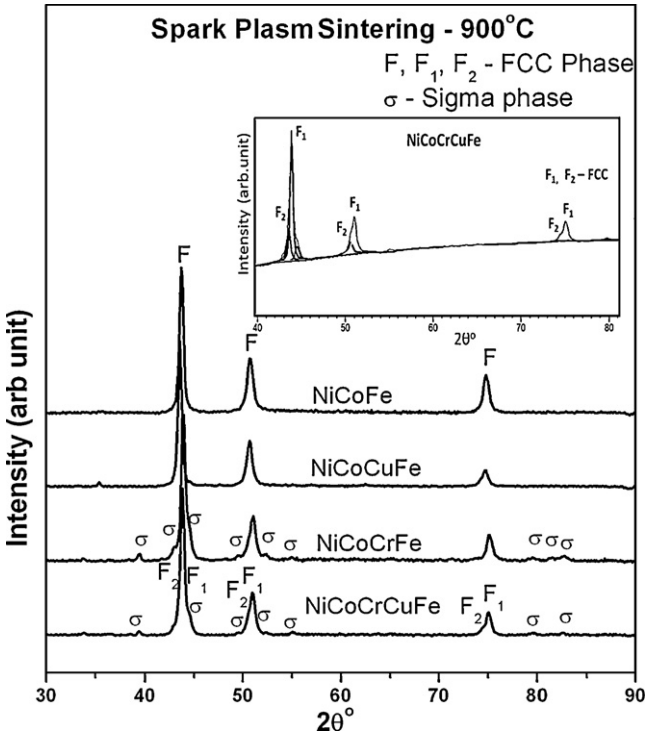

Fig. 4. XRD patterns of NiCoFe, NiCoCuFe, NiCoCrFe and NiCoCrCuFe after SPS. Inset shows the de-convoluted form of XRD peaks corresponding to NiCoCrCuFe.

Table 1
Phase evolution after MA and SPS based on XRD analysis.

HEAs	After MA	After SPS at 900 °C
AlCoCrCuFe	BCC (B) and Cu rich FCC (F_{Cu})	Ordered BCC (B2), Cu rich FCC (F_{Cu}), sigma phase (σ)
NiCoCrCuFe	FCC (F) and BCC (B_{minor})	Two FCC (F_1 and F_2), sigma phase (σ)
NiCoCrFe	FCC (F) and BCC (B_{minor})	FCC (F) and sigma phase (σ)
NiCoCuFe	FCC (F)	Two FCC (F_1 and F_2)
NiCoFe	FCC (F)	FCC (F)

Table 2
Relative density obtained for the SPS samples.

HEAs	Theoretical density (g/cm^3)	Experimental relative density (%)
AlCoCrCuFe	6.75	99
NiCoCrCuFe	8.33	94
NiCoCrFe	8.17	94
NiCoCuFe	8.64	86
NiCoFe	8.53	92

sigma phase (σ) in NiCoFe and NiCoCuFe suggests that the minor sigma phase (σ) in NiCoCrCuFe and NiCoCrFe is a Cr containing phase. A detailed summary of phases formed after MA and SPS are listed in Table 1 for comparison

3.3. Microstructural characterization after SPS

Fig. 5a and b represents back-scattered electron (BSE) images of AlCoCrCuFe at different magnifications after densification by SPS, and Fig. 5c and d represents those of NiCoCrCuFe. In both these alloy systems, a clear two-phase contrast is visible from BSE-SEM micrographs. Fig. 6a and b illustrates the spot EDS analysis on the two phases (white and grey) in AlCoCrCuFe, and the light grey and dark grey phases in NiCoCrCuFe. Black spots scattered in microstructure correspond to micro and nano porosity.

The BSE-SEM micrographs (Fig. 5a and b) together with spot EDS analysis (Fig. 6a) suggest that white phase is a Cu-rich phase and grey phase is a Cu-depleted phase in AlCoCrCuFe. Irrespective of Cu distribution, other elements are presented at near equi-atomic. Clearly, this Cu-rich phase (white) can also be correlated with the FCC (F_{Cu}) phase, and Cu-depleted phase (grey) with major BCC (B2) phase observed in XRD pattern (Fig. 3). Spot EDS analysis (Fig. 6b) on NiCoCrCuFe indicates that dark grey phase is Cr-rich phase while light grey phase is Cr-depleted phase. Atomic percentage of Ni and Cu observed to be more in Cr depleted phase than Fe and Co. However, Ni, Fe Co and Cu are observed to be distributed at near equi-atomic percentage in Cr rich phase. At lower magnification, as shown in Fig. 5c, Cr-depleted light grey phase seems to be distributed as a network like structure. However, at higher magnification (Fig. 5d), Cr-rich phase is distributed within the Cr-depleted phase. The Cr-depleted phase (light grey) can be correlated with that of FCC (F_2) phase of XRD (Fig. 3), and Cr-rich phase (dark grey) with that of FCC (F_1) and the small amount of σ phase observed in XRD pattern (which is not clearly visible in the SEM images).

Theoretical density of the alloys was calculated using rule of mixture of elemental densities and experimental density was measured using Archimedes principle. Relative density (%) is calculated with respect to theoretical density and reported in Table 2. AlCoCrCuFe shows a high relative density of 99%. However, when Al was replaced by Ni, the alloy shows a decrease in relative density to 94% under same parameters of sintering. Also, higher densification was observed in Cr containing system than systems without Cr.

Table 3
Crystallite size and lattice strain of MA and SPS samples.

HEAs	Mechanically alloyed powder		Sintered compact	
	Crystallite size (nm)	Strain (%)	Crystallite size (nm)	Strain (%)
AlCoCrCuFe	10	0.50	74	0.09
NiCoCrCuFe	7.0	1.00	27	0.14
NiCoCrFe	6.0	0.83	13	0.00
NiCoCuFe	9.0	0.73	16	0.05
NiCoFe	10	0.98	25	0.00

Table 4
Vickers hardness for HEAs.

HEAs	Hardness (HV_1)
AlCoCrCuFe	770 ± 10
NiCoCrCuFe	400 ± 10
NiCoCrFe	490 ± 10
NiCoCuFe	160 ± 10
NiCoFe	230 ± 5.0

3.4. Crystallite size and Vickers hardness

Pseudo-Voigt function was used for fitting XRD peak profile and Si standard was used for instrumental broadening correction. Crystallite size and lattice strain were calculated for the consolidated sample using Williamson–Hall method. XRD pattern profile fitting, size and strain calculation were done using Xpert Highscore plus software. Table 3 presents the crystallite size and lattice strain for mechanical alloyed powders and spark plasma sintered samples estimated using the Williamson–Hall analysis. Crystallite sizes of 6–10 nm and lattice strain of 0.5–1.0% are observed for mechanical alloyed powders. However, after SPS, lattice strain was reduced to less than 0.2% and some growth in crystallite size was observed while retaining the nanocrystallanity. Growth in crystallite size is observed to be higher in AlCoCrCuFe (10–74 nm) than in other alloy systems.

Vicker's hardness values for the spark plasma sintered samples are shown in Table 4. The highest hardness of 770 ± 10 HV is observed for AlCoCrCuFe. When Al is replaced by Ni, hardness drops drastically to 400 ± 10 HV. Further, the removal of Cu from NiCoCrCuFe brought up the hardness value to 490 ± 10 HV. However, when Cr is absent from NiCoCrCuFe and NiCoCrFe, the hardness value is observed to be very less, 160 ± 10 HV for NiCoCuFe and 230 ± 5 HV for NiCoFe.

4. Discussion

4.1. Anomalies with solid solution criteria for HEAs

The excellent work by Yeh et al. [1–6] has established that it is possible to form simple solid solutions when five or more than five elements are mixed in equi-atomic proportion. Subsequently, Zhang and Zhou [15,16] have proposed a solid solution criteria for multi-principle elemental HEAs. It's been suggested that multi-component equi-atomic HEAs are expected to form single phase solid solution, if the following conditions are satisfied: configurational entropy (ΔS_{config}) greater than or equal to 1.61R (R is universal gas constant), enthalpy of mixing (ΔH_m) in the range of $\{(-2.685\delta) - 2.54\} < \Delta H_m < \{(-1.28\delta) + 5.44$ kJ/mol$\}$ (i.e. 5 to −15 for $\delta = 4.6\%$), and atomic size difference (δ) less than or equal to 4.6% [15,16]. Thus, these parameters are calculated for the alloy systems in the present study and are listed in Table 5. It is important to note that solid solution criteria specified by Zhang and Zhou are satisfied by all the alloy systems studied in the present work. However, as summarized in Table 1, at least two phases are observed in all the

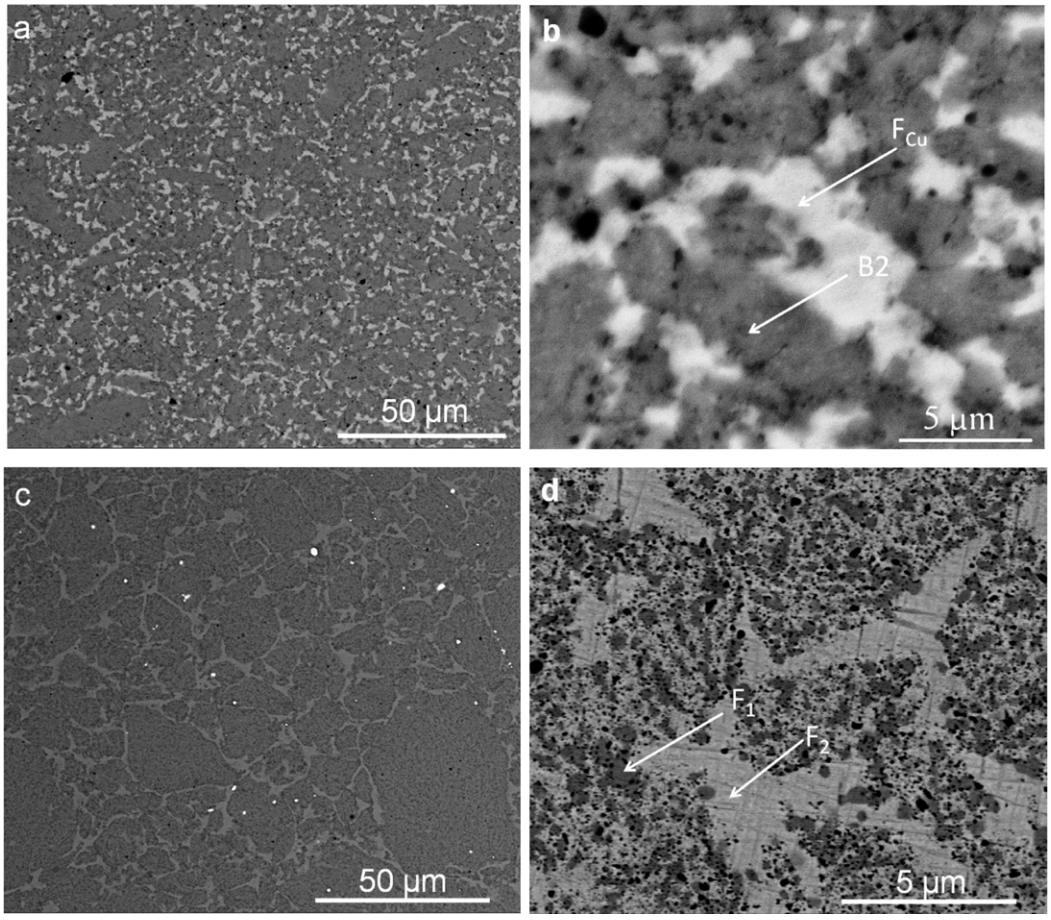

Fig. 5. The BSE-SEM images of SPS pellets: (a) and (b) of AlCoCrCuFe and (c) and (d) of NiCoCrCuFe.

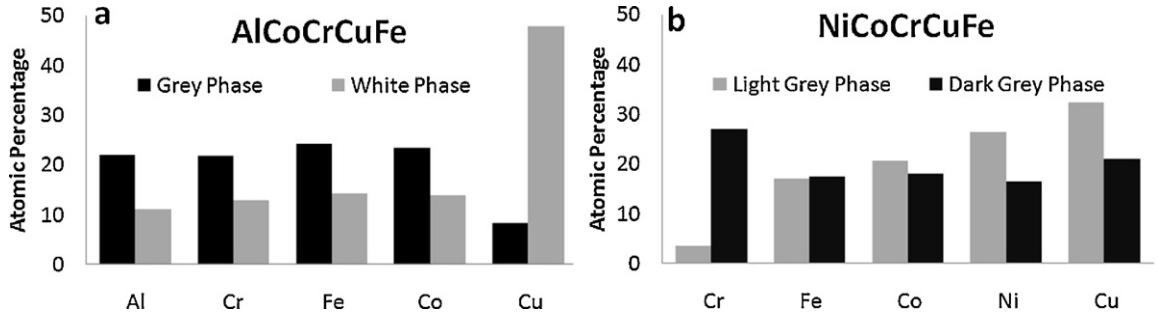

Fig. 6. Spot EDS analysis results of different regions in (a) AlCoCrCuFe and (b) NiCoCrCuFe.

Table 5
Solid solution criteria parameter values for HEAs.

HEAs	Entropy of mixing (ΔS_{mix}) (R = 8.314 J/mol K)	Enthalpy of mixing (kJ/mol) (ΔH_{mix})	Atomic size difference (%) (δ)
AlCoCrCuFe	1.61R	−2.56	4.99
NiCoCrCuFe	1.61R	3.20	1.07
NiCoCrFe	1.34R	−3.75	1.03
NiCoCuFe	1.34R	5.00	1.03
NiCoFe	1.10R	−1.33	0.76

Table 6
Enthalpy of mixing (kJ/mol) between elements.

	Al	Co	Cr	Cu	Fe	Ni
Al	–	−19	−10	−1	−11	−22
Co	−19	–	−4.0	6.0	−1.0	0
Cr	−10	−4.0	–	12	−1.0	−7.0
Cu	−1.0	6.0	12	–	13	4.0
Fe	−11	−1.0	−1.0	13	–	−2.0
Ni	−22	0.0	−7.0	4.0	−2.0	–

alloys, except in NiCoFe. Thus, it is anticipated that the solid solution criteria specified for multi-principle elemental alloys appear to be a necessary condition but not sufficient enough to predict the single phase solid solution formation in HEAs.

In addition, Cu is observed to precipitate out and such an observation is also consistent with earlier reports dealing with the alloy systems containing Cu [3,4,6,7]. The possible reasons for Cu segregation can be explained based on the enthalpy of mixing of Cu with other elements in a given alloy system. Table 6 presents the

enthalpy of mixing of the equi-atomic binary pairs of elements used in this study.

It is illustrated clearly in Table 6 that as compared to all other elements in the present alloy systems, Cu has positive enthalpy mixing with more number of elements (with Co, Cr and Fe). According to the so-called definition of HEAs [1] and based on solid solution criteria for HEAs [15,16], simple FCC phase or BCC phase with no intermediate phase is expected to form in the present alloy systems. However, in addition to Cu-rich phase precipitation during densification, sigma phase is also observed in all the alloy systems containing Cr. This sigma phase could be CoCr or FeCr intermediate phase with tetragonal structure and it was documented to be observed at the center of the phase diagrams of Cr–Co and Fe–Cr [17–19]. Previous studies on $Al_{0.5}CoCrCuFeNiTi_x$ ($x = 0–2$), $AlCo_xCrFeMo_{0.5}$ ($x = 0.5–2$) and $AlCoCr_xFeMo_{0.5}Ni$ have also shown the formation of Co–Cr σ phase [6,20,21].

In the present study, NiCoFe system has the least configurational entropy among the five alloy systems studied, however, a single phase FCC solid solution has formed after MA in this alloy, and this phase is stable even after sintering. This observation together with afore-mentioned discussion suggest that higher or lower configurational entropy alone cannot justify the formation of single phase solid solution in HEAs. Wang et al. [22] also made similar observation, and reported that configurational entropy alone is not sufficient enough to suppress the formation of Al–Ni intermetallic compound in AlCrFeCoNiCu. Also, in the present study intermetallic B2 phase formation could not be suppressed in AlCoCrCuFe alloy after SPS, although the alloy has large configurational entropy due to equi-atomic quinary composition. Thus, there is a need for devising an appropriate and valid solid solution criteria for multi-principal HEAs, and the existing criteria are insufficient to explain the present results.

4.2. Possible explanation for specific phase formation in each system

In NiCoCrCuFe alloy (Fig. 1b), a shift in the Ni peaks towards lower angles during MA is observed and all the elements are observed to be dissolving into Ni peaks with increasing milling time. The shift in the peak can be attributed to alloy formation initiated after 10 h of milling. The FCC being a closed pack structure, it may not be able to accommodate other elements without lattice expansion, and thus a shift in Ni peaks towards left. A similar behavior has been observed by Gomez-Esparza et al. in NiCoAlFeCu [14]. Lattice parameter of Ni and Cu are 3.52 and 3.61 Å, respectively. The lattice parameter of NiCoFe, NiCoCuFe, NiCoCrFe and NiCoCrCuFe estimated from the respective XRD patterns are 3.58, 3.60, 3.59 and 3.62 Å, respectively. A small increase in lattice parameter can be seen with increasing the number elements, which clearly suggests the lattice expansion and shift in Ni peaks towards left with increasing the number of elements. In contrast, no peak shift is observed in AlCoCrCuFe as the milling progresses, and all the elements except Cu are observed to be dissolving into Fe or Cr peaks. It is possible that Fe and Cr having more open BCC crystal structure, they are able to accommodate other elements without much expansion. In addition, it is also possible that some elements might expand, while others might contract the lattice and hence the lattice parameter may not show appreciable change. In addition, the fundamental peak positions of B2 phase are very close to the Fe/Cr peak positions and hence the BCC phase observed after MA could be disordered B2 phase, which after SPS reorders and shows the superlattice reflections. This reordering is caused by the annihilation of defects introduced into the structure due to high-energy ball milling.

Complete solubility of Cu is not observed in AlCoCrCuFe after MA, and subsequently Cu segregates out as a Cu-rich FCC (F_{Cu}) phase during sintering. As explained in detail in Section 4.1, the high positive enthalpy of mixing of Cu with other alloying elements could be the primary reason for such behavior. In contrast, when Al was replaced by Ni, complete solubility of Cu into the FCC (F) phase was observed during MA. This could be attributed to the fact that Cu and Ni have complete solid solubility. Complete segregation of Cu after sintering is not observed in NiCoCrCuFe. The Cr depleted FCC phase (F_2) has more at.% of Cu followed by Ni, Co and Fe are observed. Despite positive enthalpy of mixing of Cu with other elements, strong affinity of Cu and Ni prevents the complete segregation of Cu into the second FCC phase (F_2) after sintering, in contrast to Cu-rich FCC phase (F_{Cu}) in AlCoCrCuFe. Thus, in the NiCoCrCuFe alloy, the F_1 phase could be the Fe–Ni–Cr FCC phase (as observed in Ni containing steels as Ni is FCC austenite stabilizer) with some amount of Co and Cu in it. The F_2 phase in these alloys could be the Cu–Ni FCC phase.

Removal of Cr or both Cr and Cu in NiCoCrCuFe leads to formation of single FCC (F) phase after MA. However, the presence of Cu or Cr led to the formation of new FCC phase (F_{Cu}) or sigma phase (σ) after sintering, respectively. This observation suggests that MA being a non-equilibrium process facilitates the formation of metastable FCC phase. Consequently, densification at higher temperatures has resulted in more stable phases by segregation of Cu and Cr into either Cu rich phase FCC phase or Cr containing sigma phase, depending on the composition.

4.3. High strength HEAs

As explained in Section 3, MA resulted in the formation of nanocrystalline phases. It is also interesting to note that even after the sintering, the crystallite growth is not very significant (<30 nm) in all the alloys except in AlCoCrCuFe. In this connection, it is important to note that FCC is the major phase in all the systems except in AlCoCrCuFe. Crystal growth or grain growth is governed by diffusion kinetics in a given system. In general, BCC being an open structure, diffusion takes place easily as compared to close packed structure of FCC. Thus, crystal growth in Ni containing alloys (FCC phases) is sluggish in contrast to BCC structure of AlCoCrCuFe.

Although crystallite size of AlCoCrCuFe is higher among the alloys studied, it exhibits the highest hardness. There can be a combination of factors contributing to such a higher hardness in AlCoCrCuFe. Presence of ordered BCC (B2) phase together with highest density and nanocrystallinity in AlCoCrCuFe must be responsible for exhibiting higher hardness. One of the reasons for this alloy to show higher hardness than other alloys could be due to its higher density. The higher density in this alloy after SPS in comparison to the other alloys could be due to its BCC structure, which could have enhanced diffusion causing better sintering. More analysis in this regard to contribution of strength coming from various factors is underway [23]. The alloys containing FCC phase have shown lower hardness due to their solid solution (no ordered phase) and their lower density. However, it is interesting note that the hardness of NiCoCrCuFe is significantly higher than the as cast NiCoCrCuFe [3]. Further, it has been observed that addition of Cr to an alloy system increases the hardness, possibly due to the formation hard sigma phase [20,21]. The hardness obtained for NiCoCrFe and AlCoCrCuFe HEAs is higher than the mechanically alloyed and spark plasma sintered CoCrFeNiTiAl HEAs, and vacuum arc melted refractory TaNbHfZrTi HEA [13,24].

5. Conclusions

Nanostructured AlCoCrCuFe and NiCoCrCuFe HEAs are produced by MA in metastable form, and stable microstructures are obtained after SPS at 900 °C. Transformation of BCC to FCC takes place when

Al is replaced by Ni in AlCoCrCuFe. During MA, partial dissolution of Cu in AlCoCrCuFe forms a minor FCC along with BCC phase, and partial dissolution of Cr in NiCoCrCuFe forms a minor BCC phase along with major FCC phase. In AlCoCrCuFe after SPS, the Cu-rich phase precipitates out, major BCC transforms into an ordered BCC (B2) phase, and a minor sigma phase forms. A detailed characterization of phases in these alloys together with NiCoFe, NiCoCrFe, and NiCoCuFe confirms the formation of Cu and sigma phases in NiCoCrCuFe and AlCoCrCuFe. Conclusively, it has been shown that Cu precipitates out during sintering in an alloy system containing Cu, and Cr-rich sigma phase forms in a system containing Cr. Nanocrystallinity has been maintained even after sintering at 900 °C. The AlCoCrCuFe shows very high hardness of 770 ± 10 HV due to its nanocrystalline B2 structure. Alloys containing Cr exhibit higher hardness (due to σ phase) as compared to other alloys systems. Clearly, the solid solution criteria proposed for HEAs needs a revision to account for enthalpy of mixing between elements in a given alloy system.

Acknowledgement

Authors would like to thank Naval Research Board (NRB), Directorate of Naval R&D, New Delhi, India for the financial support through the project # DNRD/05/4003/NRB/190.

References

[1] J.W. Yeh, S.K. Chen, J.Y. Gan, T.S. Chin, T.T. Shun, C.H. Tsau, S.Y. Chang, Adv. Eng. Mater. 6 (2004) 299–303.
[2] C.Y. Hsu, J.W. Yeh, S.K. Chen, T.T. Shun, Metall. Mater. Trans. 35A (2004) 1465–1469.
[3] J.W. Yeh, S.K. Chen, J.Y. Gan, S.J. Lin, T.S. Chin, T.T. Shun, C.H. Tsau, S.Y. Chang, Metall. Mater. Trans. 35A (2004) 2533–2536.
[4] C.J. Tong, S.K. Chen, J.W. Yeh, T.T. Shun, C.H. Tsau, S.J. Lin, S.Y. Chang, Metall. Mater. Trans. 36A (2005) 881–893.
[5] C.J. Tong, M.R. Chen, S.K. Chen, J.W. Yeh, T.T. Shun, S.J. Lin, S.Y. Chang, Metall. Mater. Trans. 36A (2005) 1263–1271.
[6] M.R. Chen, S.J. Lin, J.W. Yeh, S.K. Chen, Y.S. Huang, C.P. Tu, Mater. Trans. 47 (2006) 1395–1401.
[7] S. Singh, N. Wanderka, B.S. Murty, U. Glatzel, J. Banhart, Acta Mater. 59 (2011) 182–190.
[8] S. Varalakshmi, M. Kamaraj, B.S. Murty, J. Alloys Compd. 460 (2008) 253–257.
[9] Y.L. Chen, Y.H. Hu, C.A. Hsieh, J.W. Yeh, S.K. Chen, J. Alloys Compd. 481 (2009) 768–775.
[10] Y.L. Chen, Y.H. Hu, C.W. Tsai, C.A. Hsieh, S.W. Kao, J.W. Yeh, T.S. Chin, S.K. Chen, J. Alloys Compd. 477 (2009) 696–705.
[11] Y.L. Chen, Y.H. Hu, C.W. Tsai, J.W. Yeh, S.K. Chen, S.Y. Chang, Mater. Chem. Phys. 118 (2009) 354–361.
[12] S. Varalakshmi, G. Appa Rao, M. Kamaraj, B.S. Murty, J. Mater. Sci. 45 (2010) 5158–5163.
[13] K.B. Zhang, Z.Y. Fu, J.Y. Zhang, W.M. Wang, S.W. Lee, K. Niihara, J. Alloys Compd. 495 (2010) 33–38.
[14] C.D. Gomez-Esparza, R.A. Ochoa-Gamboa, I. Estrada-Guel, J.G. Cabanas-Morena, J.I. Barajas-Villarruel, A. Arizmendi-Mprquecho, J.M. Herrera-Ramirez, R. Martinez-Sanchez, J. Alloys Compd. 509 (2011) 279–283.
[15] Y. Zhang, Y.J. Zhou, Mater. Sci. Forum 561–565 (2007) 1337–1339.
[16] Y. Zhang, Y.J. Zhou, J.P. Lin, G.L. Chen, P.K. Liaw, Adv. Eng. Mater. 10 (2008) 534–538.
[17] C. Allibert, C. Bernard, N. Valignat, M. Dombre, J. Less-Common Met. 59 (1978) 211–228.
[18] http://www.calphad.com/pdf/Fe_Cr(V)_Phase_Diagram.pdf (accessed 26.08.11).
[19] J. Vrestal, J. Houserova, M. Sob, J. Mining Met. 38 (3–4B) (2002) 205–211.
[20] C.Y. Hsu, W.R. Wang, W.Y. Tang, S.K. Chen, J.W. Yeh, Adv. Eng. Mater. 12 (2010) 1–2.
[21] C.Y. Hsu, C.C. Juan, W.R. Wang, T.S. Sheu, J.W. Yeh, S.K. Chen, Mater. Sci. Eng. 528A (2011) 3581–3588.
[22] Y.P. Wang, B.S. Li, H.Z. Fu, Adv. Eng. Mater. 11 (2009) 641–644.
[23] R. Sriharitha, B.S. Murty, R.S. Kottada, in prepration.
[24] O.N. Senkov, J.M. Scott, S.V. Senkova, D.B. Mircale, C.F. Woodward, J. Alloys Compd. 509 (2011) 6043–6048.